ELSEVIER

Palaeogeography, Palaeoclimatology, Palaeoecology 133 (1997) 49–68

PALAEO

High-resolution iridium, $\delta^{13}C$, $\delta^{18}O$, foraminifera and nannofossil profiles across the latest Paleocene benthic extinction event at Zumaya, Spain

Birger Schmitz [a,*], Frank Asaro [b], Eustoquio Molina [c], Simonetta Monechi [d], Katharina von Salis [e], Robert P. Speijer [a,1]

[a] *Department of Marine Geology, Earth Sciences Centre, University of Göteborg, S-413 81 Göteborg, Sweden*
[b] *Lawrence Berkeley National Laboratory, MS 195/Bldg 70, University of California, Berkeley, CA 94720, USA*
[c] *Departamento de Geologia (Paleontologia), Facultad de Ciencias, Universidad de Zaragoza, 50009 Zaragoza, Spain*
[d] *Dipartimento di Scienze della Terra, Universita di Firenze, Via La Pira 4, 50121 Firenze, Italy*
[e] *Geological Institute, Swiss Federal Institute of Technology, CH-8092 Zürich, Switzerland*

Received 4 January 1996; accepted 29 January 1997

Abstract

In the expanded upper Paleocene–lower Eocene section (≈30 m of Zone P5 sediments) at Zumaya, northern Spain, the highest occurrence of many late Paleocene deep-sea benthic foraminifera species (≈40% extinction), coincides with a transition from marl to calcite-free clay. Our high-resolution studies (chemical elements, $\delta^{13}C$, $\delta^{18}O$, calcareous nannofossils, planktic and benthic foraminifera) show that below the marl–clay transition there is a 40–50 cm thick interval (corresponding to 10–20 kyr) containing a detailed record of a gradual succession of faunal and geochemical events culminating in the benthic extinctions. Planktic foraminiferal and nannofossil changes (e.g., the onset of demise in *Fasciculithus* genus) occur a few meters below the marl–clay transition. In the limestone 50 cm below the base of the clay, a prominent glauconite maximum indicates that sea-floor oxygenation suddenly decreased. Glauconite continues to be common until the onset of clay deposition. A whole-rock negative $\delta^{13}C$ shift (1.6‰), most likely reflecting an original sea-water trend, is gradually developed over the 40 cm of greenish brown marls immediately below the clay. At the base of these marls there is a small, significant iridium anomaly of 133 ppt Ir compared with an average background of 38 ppt. In the marls the demise of the *Fasciculithus* species accelerates, *Gavelinella beccariiformis* becomes extinct, and the abundance of *Acarinina* species begins to increase. The superjacent 4 m of clay is devoid of original calcite in its lower part and has a low calcareous content higher up. At calcareous levels in the clay an unusual planktic foraminifera fauna occurs, dominated by *Acarinina* species. When marl deposition returns, $\delta^{13}C$ gradually increases and then stabilizes at values about 0.5‰ lower than before the isotopic excursion. The $\delta^{13}C$ excursion spans in total 5 m, probably corresponding to 200–400 kyr. The fasciculiths disappear shortly after the stabilization of $\delta^{13}C$.

Here we also present a whole-rock $\delta^{13}C$ profile through the entire Paleocene section at Zumaya. The profile is very similar to previous profiles registered in well preserved deep-sea material, suggesting that whole-rock $\delta^{13}C$ at Zumaya can be used for correlation.

* Corresponding author. Fax: +46 31 7734903. E-mail: birger@gvc.gu.se
[1]Present address: University of Bremen, FB 5, Geosciences, Box 330440, 28334 Bremen, Germany.

PII S0031-0182(97)00024-2

The origin of the Ir anomaly ≈40 cm below the benthic extinction event is enigmatic. It may be impact-related; however, the clearly gradual sequence of environmental events in the 50 cm below the dissolution clay, are more readily reconciled with changing oceanic circulation and palaeogeographic change, possibly in connection with volcanism, than with an instantaneous impact. The small Ir anomaly may reflect such volcanism, sea-water precipitates, or a small impact event, possibly unrelated to the palaeoenvironmental change. © 1997 Elsevier Science B.V.

Keywords: iridium; stable isotopes; upper Paleocene; benthic taxa; foraminifera; mass extinctions

1. Introduction

The largest extinction event affecting the deep-sea benthic foraminiferal fauna during the past 90 million years occurred near the end of the Paleocene. About 35–50% of the deep-sea benthic species became extinct at this event (Tjalsma and Lohmann, 1983; Thomas, 1990; Kennett and Stott, 1991; Pak and Miller, 1992; Kaiho, 1994). High-resolution studies at ODP Hole 690B, drilled at Maud Rise off Antarctica, show that the main extinction phase was rapid (<3 kyr) and occurred at the beginning of a short period (<100 kyr) of conspicuously anomalous deep-water conditions (Kennett and Stott, 1991). The temperatures of Maud Rise bottom waters at 2,100 m palaeodepth rose from 9°C to 16°C, and the water column experienced a 2–4‰ negative shift in $\delta^{13}C$ composition. This has been attributed to a shift in the source region of global deep-water from the high latitudes to subtropical regions, in connection with a high-latitude warming event (Kennett and Stott, 1991). It is hypothesized that warm, saline surface water in the subtropical net evaporation zones began to spread over the global sea floor, leading to benthic faunal turnover. Planktic and shallow-water benthic foraminifera faunas also experienced turnovers, but to a lesser extent (Canudo et al., 1995; Lu and Keller, 1995; Speijer et al., 1996a, Speijer et al., 1996b). On the southern Tethyan shelf a long-lasting (>1000 kyr) biotic and environmental change was triggered, reflecting possibly a change in oceanic circulation or wind patterns (Schmitz et al., 1996c).

Some kind of physical event must have triggered these abrupt oceanic changes in the latest Paleocene. It could have been a violent volcanic event that emitted gases, inducing a short-term greenhouse climate, or volcanism may have changed palaeogeography, eventually leading to perturbations in oceanic circulation. The latter is a particularly likely scenario, since modelling experiments indicate that deep-water source regions may be highly sensitive to changing palaeogeography (Barron and Peterson, 1991). For example, an early phase of the volcanism in connection with the opening of the northernmost Atlantic (Knox and Morton, 1988; Eldholm and Thomas, 1993) may have triggered such a change. Alternatively, the impact of an extraterrestrial body could have interfered with the evolution of life, just as at the Cretaceous–Tertiary (K–T) boundary, some ten million years earlier. At a first consideration, this alternative appears unlikely, considering that the two events affected primarily two completely different oceanic faunal realms. During the K–T boundary event the planktic realm was severely affected, whereas the deep-sea benthic fauna only experienced minor changes (Thomas, 1990; Thomas and Shackleton, 1996). Very little is known, however, about the possible environmental effects of different kinds of medium to large impacts.

In order to find traces of any physical event that may have triggered the sequence of events leading to the latest Paleocene benthic foraminiferal extinction event, we performed detailed high-resolution, centimetre-scale, geochemical studies ($\delta^{13}C$, $\delta^{18}O$, Ir, Fe, Sc, Cr, Se and other elements) in the uppermost Paleocene parts of the Zumaya section in northern Spain. We have also refined the biostratigraphic (benthic and planktic foraminifera and nannofossils) frame for this interval.

The Zumaya section contains one of the most

expanded and biostratigraphically complete Paleocene–Eocene transitions known, with over 40 m of section representing planktic foraminiferal zones P5–P6b (lowermost part) (Canudo et al., 1995). The section is considered to be one of the candidates for being elected as the Paleocene–Eocene (P–E) boundary stratotype (Canudo and Molina, 1992). At Zumaya, the benthic extinction event, characterized by a 38% extinction of smaller benthic foraminifera, including *Gavelinella beccariiformis,* closely coincides with deposition of a clay interval, indicating strong $CaCO_3$ undersaturation in connection with the extinction event (Canudo et al., 1995; Ortiz, 1995).

2. Lithostratigraphy

The upper Paleocene and lower Eocene part of the Zumaya section probably formed in a middle or lower bathyal environment (Pujalte et al., 1993; Canudo et al., 1995). The lithology in the 15 m interval below the benthic extinction event is dominated by grey marls (Fig. 1). A prominent, 0.7 m thick, grey limestone bed interrupts the marl succession. The limestone is overlain by about 40 cm of marl, followed by a mainly reddish brown clay interval, 4 m thick. The clay interval is devoid of original calcite in its lower 1 m (Fig. 2). In its upper 3 m it is slightly calcareous (10–20%) at

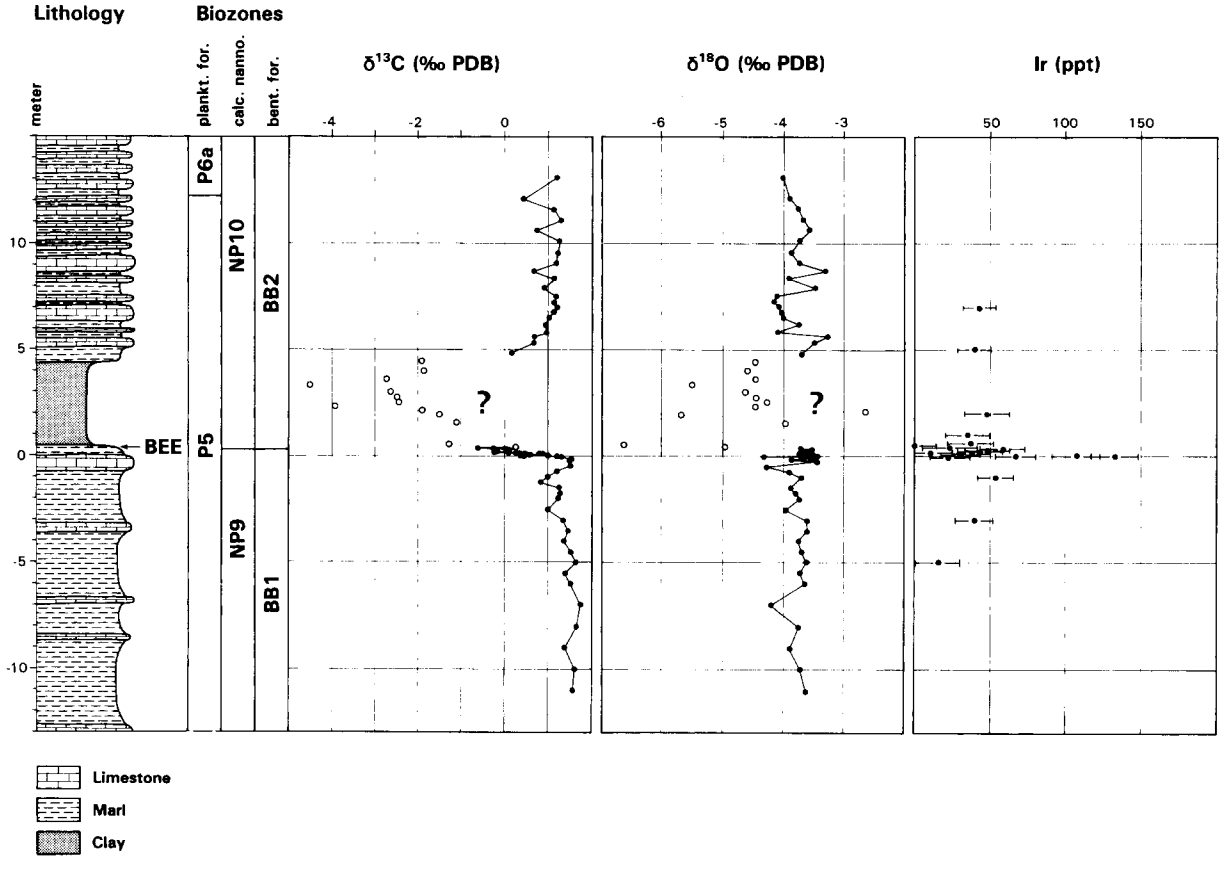

Fig. 1. Lithostratigraphy, biostratigraphy and chemostratigraphy across the Paleocene–Eocene transition at Zumaya. *BEE* = benthic extinction event. Many of the isotopic results in the dissolution clay (circles) may represent diagenetic signatures rather than original sea-water values. Error bars on the Ir results reflect analytical uncertainty (see Schmitz and Asaro, 1996). The position of the P–E boundary is presently being revised within the activities of the P–E Boundary Stratotype Working Group. The boundary will most likely be defined at a level in the interval between the BEE and the P5/P6a boundary.

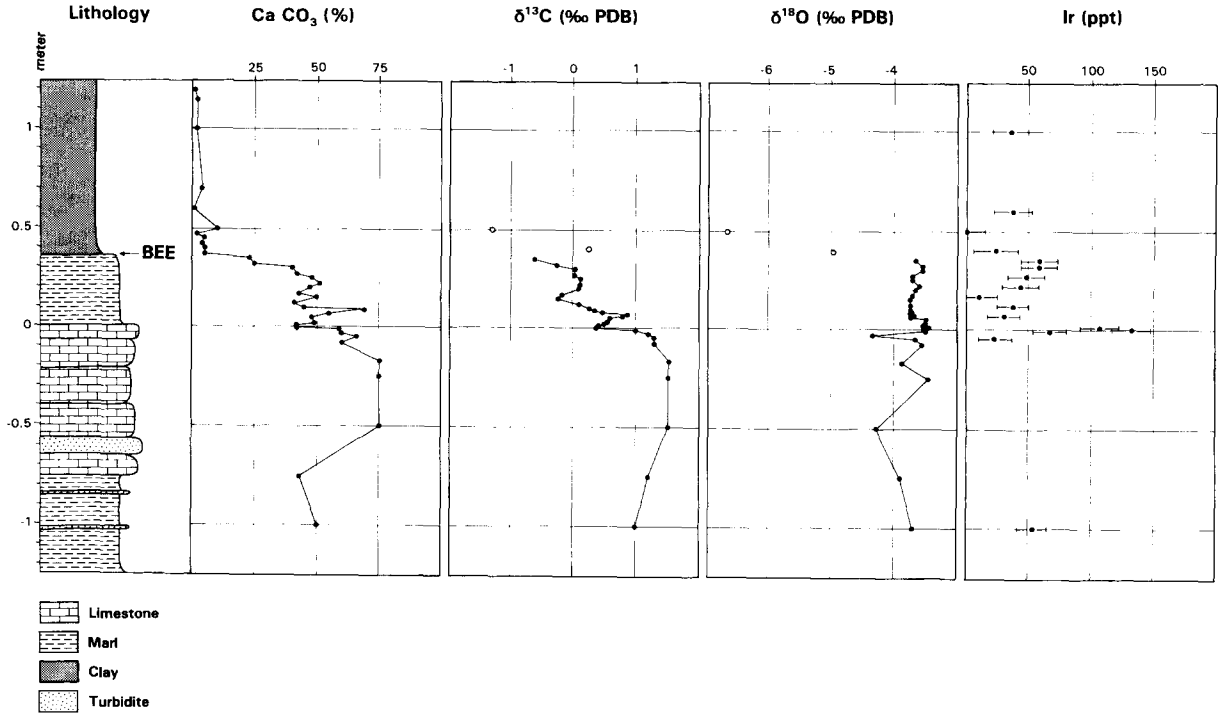

Fig. 2. High-resolution lithostratigraphy and chemostratigraphy across the benthic extinction event at Zumaya. The highest occurrence of many Paleocene benthic foraminifera occurs at the base of the clay interval. The lower part of the clay only contains agglutinated benthic foraminifera tests, therefore it can only be assumed that the highest occurrence of the benthics corresponds to the time of their extinction. For further information see caption of Fig. 1.

several levels, and contains some dissolution-resistant calcareous microfossils. Upwards the calcareous clay passes gradually into marls and thereafter limestones (Fig. 3). The upper 9 m of the section studied is dominated by limestone with marl intercalations.

The lithostratigraphy of the interval across the transition from marl to clay, including the interval down to 1.5 m below this transition, is displayed in more detail in Fig. 2. A turbidite, 8 cm thick, is found in the lower part of the grey limestone bed below the benthic extinction event. Such turbidites are common throughout the Zumaya section (in particular in the Eocene part), but rare in the 28 m thick interval studied here. The grey limestone bed is a conspicuous marker that can also be traced into other sections in the Basque country. In the topmost 10 cm the limestone is very glauconitic, with abundant glauconized foraminifera tests. The overlying 30–40 cm of marls are also relatively rich in glauconite. The marls have a greenish brown appearance, quite different from the grey marls below the limestone bed. The transition from marl to clay is gradual over about 10 cm. The clay interval is dark brown in its lower part, alternating grey and red higher up, and is predominantly reddish brown throughout its upper part.

The basal 1 cm interval of the 30–40 cm of greenish brown marls, between the limestone bed and the clay, attracted our interest. This layer differs from the overlying marl interval by a more greyish colour. The layer can only be recovered in exposures where no sliding at the transition between limestone and marl has taken place. In strongly weathered exposures the topmost 1 cm of the glauconitic limestone may be confused with the basal, 1 cm thick, grey marl. In this study we use the base of the grey marl as the zero level in

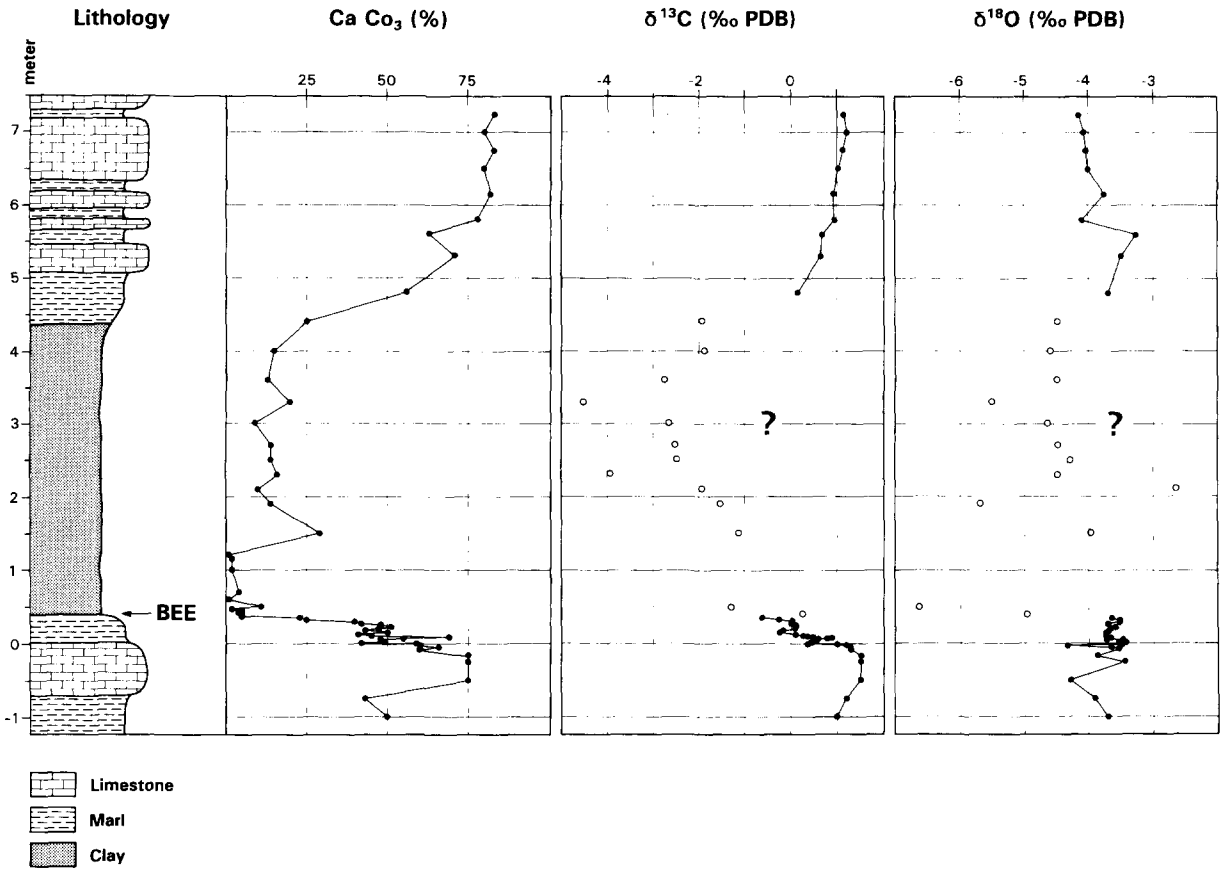

Fig. 3. Lithostratigraphy and chemostratigraphy across the dissolution clay interval at Zumaya. For further information see caption of Fig. 1.

our profile. The level corresponds to the 18 m level in the profile established by Canudo et al. (1995). The lithological succession across the interval displayed in Fig. 2 appears to be continuous. Although studied in detail, no unconformities have been found.

3. Materials and methods

3.1. Chemical analyses

Samples were collected at San Telmo Beach (see detailed map in Canudo et al., 1995). Preliminary chemical analyses were performed on samples collected in 1992. Resampling of crucial intervals took place in 1994 and 1995. When collecting the samples for iridium analyses, all direct contact between metal tools or other noble-metal bearing objects and the sample surfaces were avoided. Sample resolution varies between 1 and 5 cm over the most important intervals across the benthic extinction event. The resolution of the background record is 25 cm for stable isotopes and 1–2 m for chemical elements. Here we also present a high-resolution $\delta^{13}C$ isotopic profile across 180 m of the uppermost Maastrichtian to lowermost Eocene section at Zumaya. About 360 samples were analyzed for this profile, with, in general, 0.5 m sample spacings.

Stable isotopic analyses were performed on bulk samples. Throughout almost the entire Paleocene

part of the Zumaya section traces of foraminifera occur only as internal molds or recrystallized tests infilled with diagenetic calcite. Under such circumstances bulk samples may give more meaningful $\delta^{13}C$ values than the foraminifera (see discussion in later section). The stable isotope analyses were performed with a VG Prism Series II mass spectrometer attached to an Isocarb automated carbonate preparation system. All values are expressed as per mil differences with respect to the PDB standard. The mean values and standard deviations of twelve analyzed NBS-19 standards are 1.96 ± 0.02‰ for $\delta^{13}C$ and -2.16 ± 0.04‰ for $\delta^{18}O$.

Chemical element (Ir, Fe, Sc, Ni, Co, Se, Sb, Cr, Rb, Cs, Ce, Hf, and Th) concentrations were analyzed with the Luis W. Alvarez–Iridium Coincidence Spectrometer (LWA–ICS) at the Lawrence Berkeley National Laboratory. The LWA–ICS has been constructed specially for high-sensitivity routine Ir analyses in geological samples (see Michel et al., 1991). The coincident emissions of two gamma rays, 316.5 keV of ^{192}Ir and 468.1 keV of ^{192}Ir, from neutron-bombarded samples are measured simultaneously in the LWA–ICS. The coincidence technique permits a much better discrimination of Ir-related gamma rays from background radiation than conventional single gamma-ray measurements. For details on analytical procedures and error estimates see Schmitz and Asaro (1996). Calcite content of the whole-rock samples was determined by calcium titration with E.D.T.A.

3.2. *Palaeontological studies*

Calcareous nannofossil and benthic foraminifera studies were performed on splits of some of the samples that were used for the chemical analyses. Semi-quantitative abundances of calcareous benthic foraminifera from sieving residues (>125 μm) were determined in the interval spanning the benthic extinction event. Several thousands of specimens were studied in each sample. Calcareous nannofossils were studied in smear slides with the light microscope. Planktic foraminifera have previously been studied by Canudo and Molina (1992) and Canudo et al. (1995). Here we add a few more detailed observations.

4. Chemical results

4.1. *$CaCO_3$, $\delta^{13}C$, and $\delta^{18}O$ distributions*

The results of the $CaCO_3$ and isotopic measurements across the P–E transition are displayed in Figs. 1–3. The isotopic results have been plotted in two categories: those for the clay interval and those for the marls–limestones above and below. We consider the results for many of the calcareous-poor samples from the clay interval to be of questionable reliance.

Calcite concentrations lie typically at 75–80% in the limestones and 40–50% in the marls. In the marls between +0.30 and 0.35 m calcite falls to 25% (Fig. 2). At +0.35–0.40 m calcite drops to 5%. In the lower 1 m of the clay interval calcite concentrations lie typically in the range 0–5%. In the upper 3 m there are many horizons with 10–20% calcite (Fig. 3). Examination of sieving residues (>63 μm) from the clay interval reveals common diagenetic calcite.

The $\delta^{13}C$ record shows a relatively stable pattern throughout the 11 m interval below the zero level, with most values in the range 1–1.7‰ (Fig. 1). From the topmost few centimetres of the limestone and across the 30–40 cm of marls immediately below the benthic extinction event, $\delta^{13}C$ shows a negative shift on the order of 1.4–1.8‰ (Figs. 2 and 3). From values around 1.2‰ in the uppermost few centimetres of the limestone, $\delta^{13}C$ falls to values in the range −0.2‰ to −0.6‰ in the marl interval between +0.30 and 0.35 m. In the poorly calcareous parts of the overlying clay interval $\delta^{13}C$ values continue to fall (except for the +0.35–0.40 m sample), reaching extremely negative values of −3.9‰ to −4.5‰ at some levels in the interval 2–3.3 m above the zero level (Fig. 3). In the marls above the dissolution clay $\delta^{13}C$ returns gradually to more positive values and thereafter, throughout the overlying 8 m of marl–limestone, fluctuates around 1‰ (Fig. 1).

The $\delta^{18}O$ values are relatively stable throughout the marl and limestone parts of the section, with

most values in the range −3.5‰ to −4‰ (Figs. 1–3). In the clay interval, however, $\delta^{18}O$ shows a widely scattered distribution, ranging between −2.6‰ and −6.6‰. The wide scatter indicates that diagenesis may have severely affected the original isotopic signals in this part of the section.

The $\delta^{13}C$ results across the entire Paleocene section are displayed in Fig. 4. At the K–T boundary there is a short-term 1.5‰ negative shift in $\delta^{13}C$, followed by a 0.7‰ positive shift in the earliest Danian (up to 7 m above the K–T boundary). The isotopic values show a slightly falling trend, from 1.8‰ to 1.6‰ through the Danian up to the Danian–Selandian (D–S) boundary (≈NP4–NP5 boundary) at around +60 m. Single, more negative values also occur in the Danian. At the D–S boundary there is a well developed (over 6 m) gradual, 1‰ negative $\delta^{13}C$ anomaly (see Schmitz et al., 1996b). A rapid increase in $\delta^{13}C$ occurs in the lower Selandian from +60 m to +75 m. The values increase by 1.9‰, from 0.6‰ to 2.5‰. The $\delta^{13}C$ values continue to increase, but more gradually, to peak values of 3.1‰ at +115 m in the Thanetian (NP7–NP8). Over the following 50 m, up to immediately below the benthic extinction event, $\delta^{13}C$ gradually falls by about 2‰. In connection with the extinction event $\delta^{13}C$ shows a rapid 1.5–2‰ decrease, as discussed above.

4.2. Chemical element distributions

In the interval where the benthic extinction event takes place no anomalous Ir values were found (Figs. 1 and 2). The values in this interval lie close to the mean value, 38 ppt (parts per trillion), for 19 of the 21 samples (excluding the two from the grey layer, see below) analysed in this study. This mean value is similar to the Ir value, ≈50 ppt (or 0.05 ppb), suggested for average continental crust (Wedepohl, 1995). In the 1 cm thick grey layer at the base of the greenish brown marls, below the benthic extinction event, a small Ir anomaly exists. One sample from this layer, collected in 1992, gave a value of 107±16 ppt Ir. In 1994 the layer and adjacent parts of the section were resampled in greater detail and at a slightly different position in the exposure. An Ir value of 133±15 ppt was obtained for the grey layer, whereas the adjacent samples gave typical background Ir values. A renewed detailed sampling in 1995 resulted in an Ir value of 143±22 ppt for the grey layer, confirming that this Ir anomaly is reproducible.

The scandium (15 ppm)-normalized distributions of iridium and 11 other elements across the benthic extinction event are displayed in Fig. 5 (see Schmitz, 1988, as regards element normalization procedures). Scandium in sediments is usually almost exclusively associated with the aluminosilicate fraction, and therefore Sc-normalization of element abundances removes any effects on element distribution patterns from diluting components such as, for example, biogenic calcite or silica. The Sc-normalized Ir (i.e., Ir*) pattern shows the same conspicuous anomaly in the grey layer as the non-normalized data. The highest Ir* concentration measured in the layer is 157 ppt, compared to an average value of 51 ppt for the rest of the section. The Fe* concentration in the grey layer is 3.4%, which is somewhat lower than the average value (3.9%) for the entire section. In the sample 5 cm below the grey layer, however, there is a Fe* peak of 8.2%. In addition, Co* shows a peak value, 53 ppm, in this layer, compared to an average of 18 ppm for the rest of the section. In the 1 cm interval below the grey layer Co* falls to 40 ppm, and in the grey layer Co* shows concentrations of 21–28 ppm, near the average for the section. The Ni* content in the grey layer and in the 5 cm thick interval just below this is higher than in the rest of the section. The average Ni* concentration in the section is 58 ppm. The highest value, 113 ppm, is measured in one of the two samples from the grey layer. In the other sample from the grey layer the Ni* content is 68 ppm (i.e., close to the average value). Apparently, Ni* is heterogeneously distributed in the grey layer. The two samples in the 5 cm interval below the grey layer show Ni* values of 88 and 104 ppm. The Fe*, Ni*, and Co* enrichments in the interval just below the grey layer are most likely somehow related to the extreme abundance of glauconized foraminifera tests in the interval. It is notable that, in the grey layer, Fe* and Co* show low concentrations, similar to average concentrations for the entire section. This is consistent

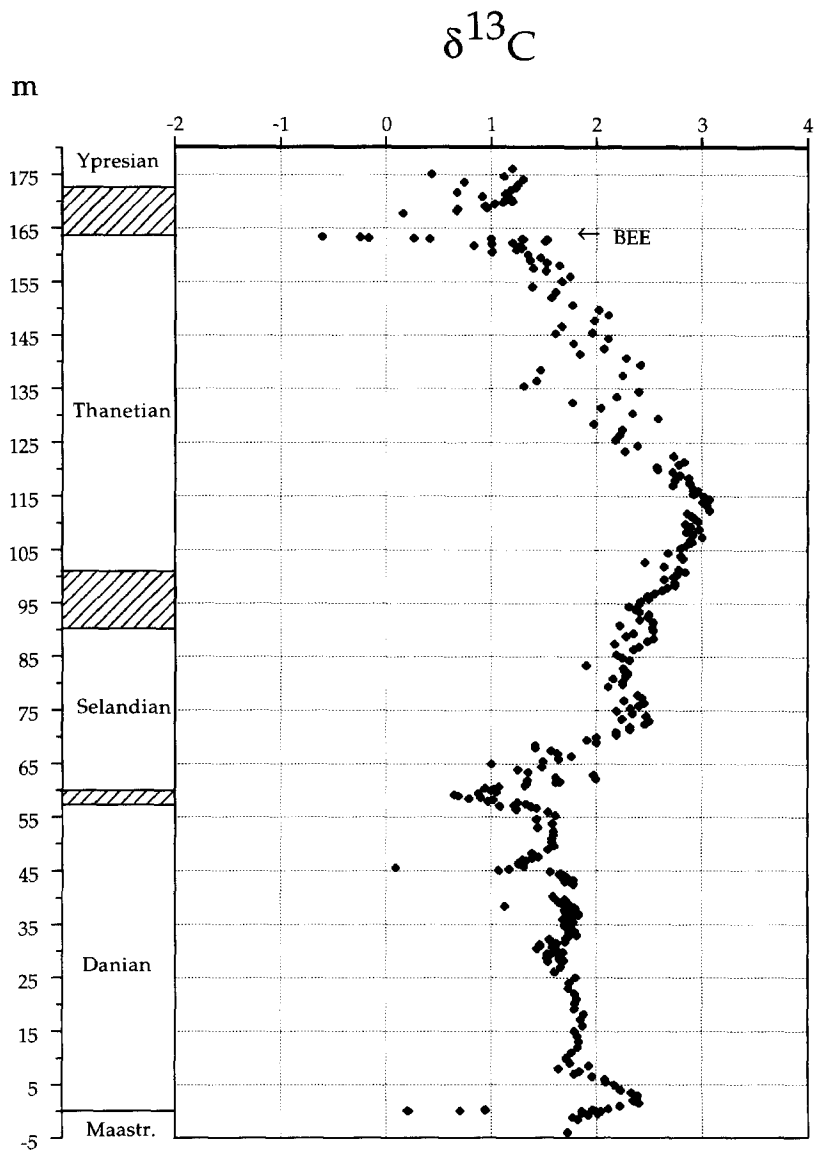

Fig. 4. Whole-rock carbon isotopic curve spanning the uppermost Maastrichtian to the lowermost Eocene at Zumaya. Hatched areas indicate intervals where stage boundaries may be defined (after Schmitz et al., 1996b). For details on biostratigraphy in the Paleocene section at Zumaya, see Molina (1994) and Schmitz et al. (1996b).

with absence of any anomalous amounts of pyrite or glauconite in the layer. Ir*, on the other hand, shows no enhancement compared with background in the strongly Fe*- and Co*-enriched sample 5 cm below the grey layer. There is thus a stratigraphic offset of 6 cm between the Ir* and the Fe* and Co* abundance peaks.

The remaining elements (Se*, Sb*, Cr*, Rb*, CS*, Ce*, Hf*, and Th*) show no unusual concentrations or anomalous abundance peaks in any of the samples analyzed. In particular, neither Se* nor Sb* show any peak concentrations in the Ir-enriched grey layer (see later discussion).

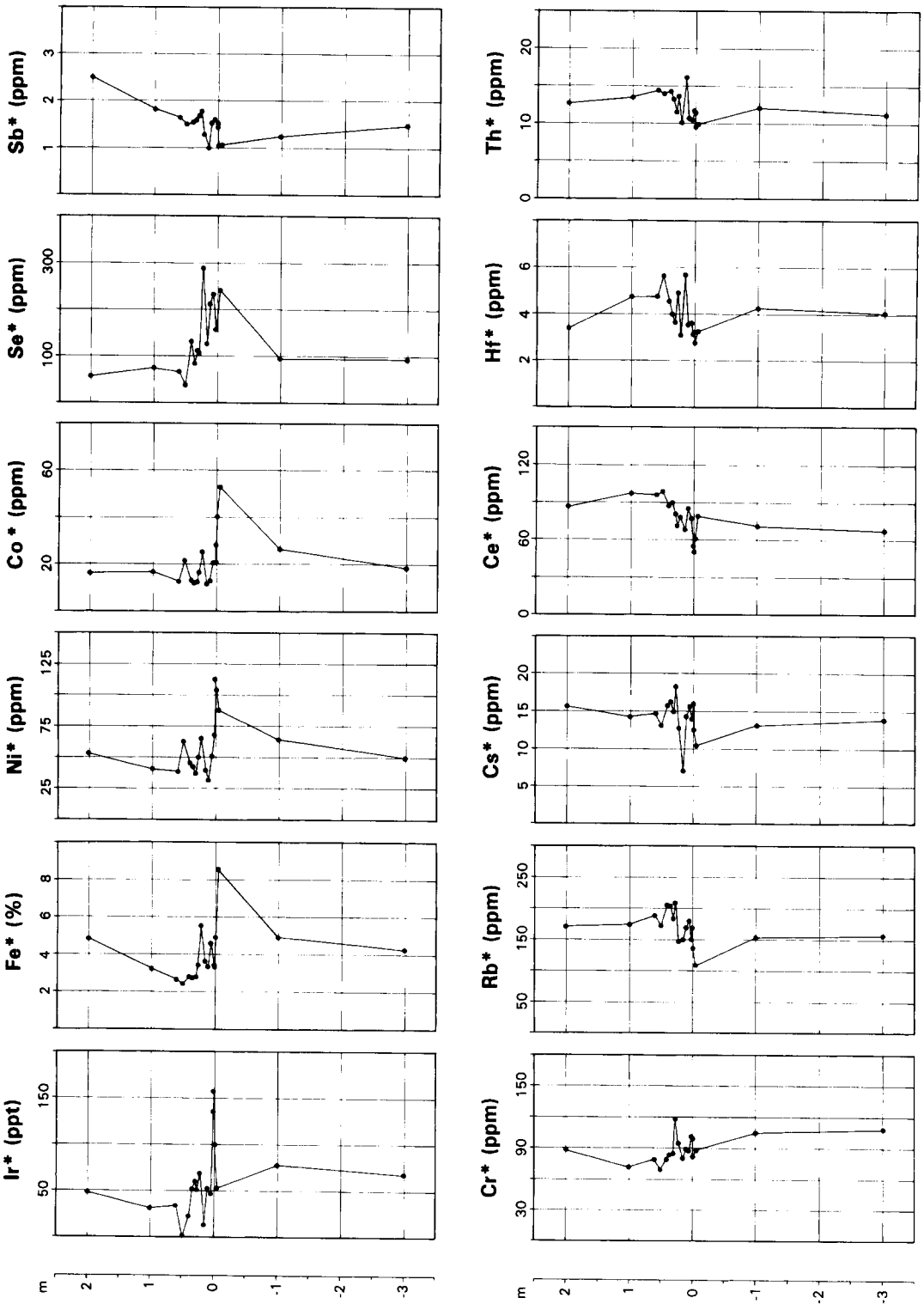

Fig. 5. Scandium (15 ppm)-normalized element distributions across the benthic extinction event at Zumaya.

5. Biostratigraphic frame

5.1. The benthic foraminiferal record

The highest occurrence (HO) of the majority of the typical late Paleocene benthic foraminifera species occurs near or at the transition from marl to clay (see later section). Because of the coincidence with calcite dissolution it is not certain that the foraminiferal highest occurrences really reflect the benthic extinction event. It appears likely, however, that the changes that led to calcite dissolution also led to extinction of the benthic foraminifera. At ODP Hole 690B, calcite dissolution and extinction clearly coincide (Kennett and Stott, 1991).

Twenty-two predominantly cosmopolitan taxa (e.g. *Cibicidoides velascoensis, Coryphostoma midwayensis, Osangularia velascoensis,* and *Pullenia coryelli)* disappear at or just below the base of the clay interval (Fig. 6). Most of these taxa are known to have become globally extinct, more or less simultaneously, at the end of the Paleocene (see overview in Speijer et al., 1996b). The highly diverse benthic fauna (40–55 taxa per sample) is fairly stable up to the base of the clay. Most

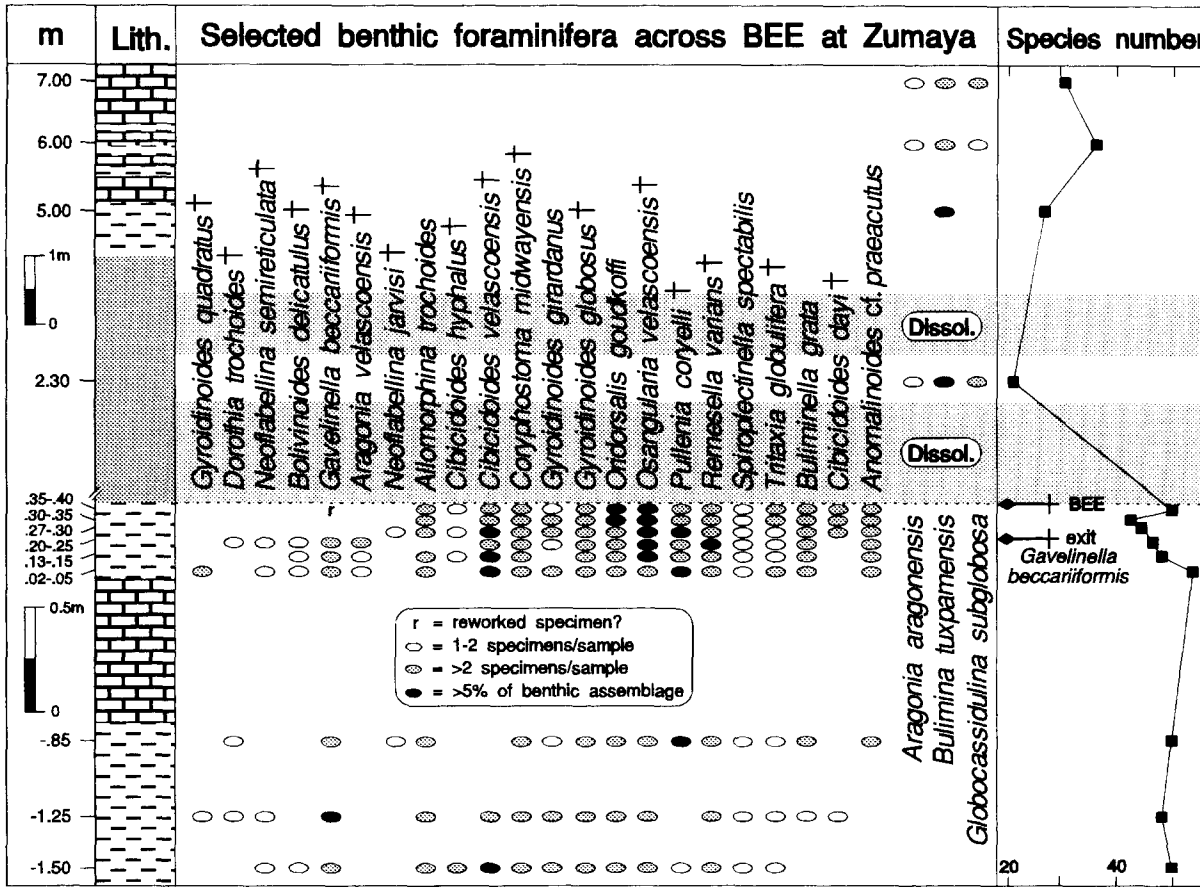

Fig. 6. Benthic foraminiferal distributions across the benthic extinction level. At Zumaya the extinction of *G. beccariiformis* precedes the benthic extinction level, which is marked by a large number of simultaneous exits of cosmopolitan deep-sea taxa at the base of the clay bed. The highest occurrence of *G. beccariiformis* was encountered 15 cm below the clay. Taxa marked by a cross became globally extinct during the benthic extinction event (see overview in Speijer et al., 1996b). Note the change of scale at the base of the clay interval.

common taxa are present up to the uppermost sample below the clay (+0.35–0.40 m). Rare taxa with a more scattered distribution (in most cases only 1 or 2 specimens per sample) disappear further below the base of the clay. The range of *Gavelinella beccariiformis* displays the only prominent exception to this general pattern. This species is consistently present (common to frequent) in the section up to 15 cm below the marl–clay transition (i.e., up to 0.25 m above the zero level); it is absent in the samples between +0.27 m and +0.35 m, whereas scanning through some 10,000 benthic specimens revealed only one specimen of *G. beccariiformis* in the sample from the +0.35–0.40 m interval. Probably this single specimen has been reworked. At least locally, *G. beccariiformis* may have become extinct earlier than the taxa it is usually associated with in deep-sea faunas.

Although a large number of taxa became extinct, they were replaced by a minor suite of newly appearing taxa (excluding scattered occurrences of some rare taxa), such as *Aragonia aragonensis, Bulimina tuxpamensis* and *Globocassidulina subglobosa.* The impoverished fauna after the benthic extinction event (20–35 taxa per sample) is largely composed of survivor taxa, such as *Nuttallides truempyi* (up to 70% of the total benthic fauna), *Abyssamina quadrata, Anomalinoides spissiformis,* and *Bulimina trinitatensis.* Similar post-extinction assemblages dominated by *N. truempyi* and with high numbers of *Abyssamina quadrata* have been found in many North and South Atlantic lower bathyal (>1000 m) to abyssal localities (Tjalsma and Lohmann, 1983; Pak and Miller, 1992; Thomas and Shackleton, 1996).

Our results are generally in good agreement with those of Ortiz (1995), who performed a quantitative analysis on a more expanded profile of the Zumaya section but included only two samples from the critical interval just below the clay. Ortiz places the extinction event above the highest occurrence of *G. beccariiformis* and *P. coryelli* and some other common taxa, but below the highest occurrence of common taxa such as *Gyroidinoides globosus, O. velascoensis,* and *Remessella varians.* Our higher resolution data of this interval indicate that *G. beccariiformis* is the only taxon amongst these with an early extinction. Many other taxa disappeared simultaneously at the base of the clay. The reduced number of species in Ortiz's highest sample below the clay probably results from the relatively small total number of benthic specimens (225) present in that sample. Our data, which are based on a much larger sample size, support a major diversity decrease above the base of the clay, not below it (Fig. 6). The prominent diversity decrease across the extinction is a globally recognized feature (Thomas and Shackleton, 1996, and references therein).

5.2. Planktic foraminiferal record

A new planktic foraminiferal biozonation has been proposed based on the coincidence of the highest occurrence of *Igorina laevigata* with the benthic extinction event (Fig. 7; Canudo and Molina, 1992; Canudo et al., 1995). This coincidence has been observed at Zumaya and other Spanish sections, such as Caravaca (Molina et al., 1994), and Alamedilla (Arenillas and Molina, 1996). In this new biozonation the *Morozovella velascoensis* Zone of Bolli et al. (1985) has been divided into two parts, with the top of the lower part at the HO of *I. laevigata.* The detailed resolution accomplished in the present study shows that *I. laevigata* ranges up to the uppermost sample below the clay in the Zumaya section. Applying the biozonation of Berggren et al. (1995), the interval studied corresponds to the P5 and P6a zones, with the benthic extinction event in the middle part of P5 (Canudo et al., 1995).

At Zumaya the *I. laevigata* Zone is represented by about 18 m and the new restricted *M. velascoensis* Zone by 12 m. This implies an expanded section compared with other continuous sections, such as Alamedilla in southern Spain, where the thicknesses are 7 m and 6 m, respectively (Arenillas and Molina, 1996).

The planktic foraminifera faunal turnover across the P–E transition at Zumaya (Canudo and Molina, 1992; Canudo et al., 1995; Molina et al., 1996) is characterized by the disappearance of *I. laevigata, A. hispicidaris, I. albeari* and *M. acutispira.* A few new species instead appeared: *A. berggreni, Truncorotaloides quetra, Muricoglobigerina angulosa,* and *Subbotina pseudoeocaena.* The most conspicuous change in planktic foraminiferal fauna, however, is the strong increase

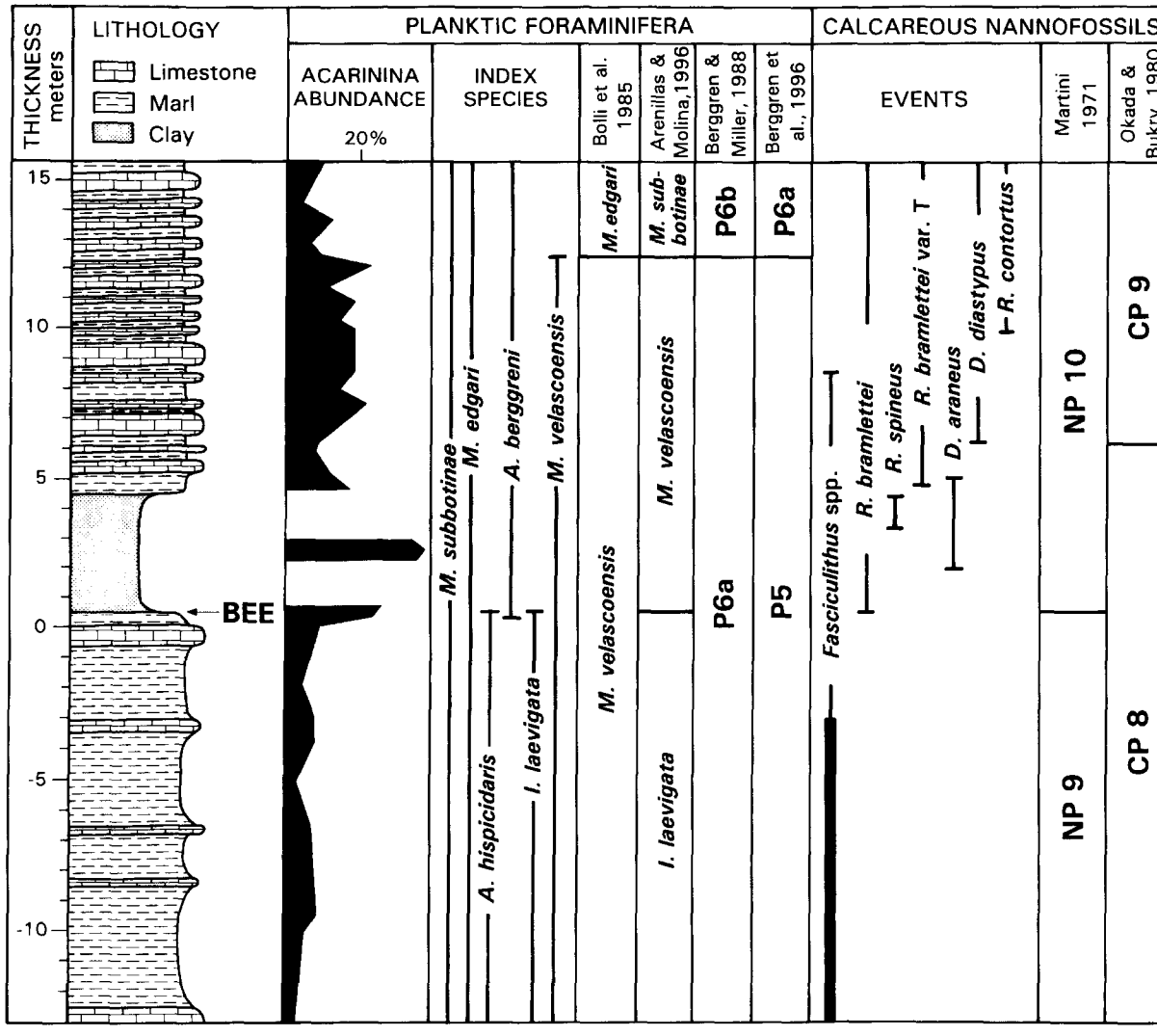

Fig. 7. Planktic foraminiferal and calcareous nannofossil biostratigraphy across the Paleocene–Eocene transition (see caption of Fig. 1) at Zumaya (with data from Martini, 1971; Okada and Bukry, 1980; Bolli et al., 1985; Berggren and Miller, 1988; Arenillas and Molina, 1996; Berggren et al., 1995).

in the relative abundance of *Acarinina*, reaching the highest values just above the benthic extinction event in the slightly calcareous middle–upper part of the dissolution clay. A similar increase in *Acarinina* coincident with the extinction event has also been found in another Spanish section (Arenillas and Molina, 1996) and in Egypt and ODP Hole 865, representing low-latitude conditions (Speijer and van der Zwaan, 1994; Speijer et al., 1996a; Kelly et al., 1996). At Zumaya, the *Acarinina* (particularly *A. wilcoxensis*) increase is already apparent at the +0.2 m level in the greenish brown marls just below the benthic foraminiferal extinction (Fig. 7; Canudo et al., 1995).

5.3. Calcareous nannofossil record

Calcareous nannofossils show a great turnover with several lowest (LO) and highest (HO) occurrences over the interval from about 2 m below to

about 6 m above the benthic extinction event (Fig. 7; Monechi and Angori, 1996). There is no drastic change, however, right across the Ir maximum at the zero level in the profile. A turnover in the calcareous nannoflora has also been recognized at many other sites (El Mamoune and Martinez-Gallego, 1995; Bralower and Mutterlose, 1995; Bybell and Self-Trail, 1995; Angori and Monechi, 1996).

The sediments below the marl to clay transition interval are characterised by a diverse coccolith assemblage including both common *Discoaster, Fasciculithus* and holococcoliths, and very rare *Rhomboaster bramlettei* and *R. intermedia.* The diversity and the abundance of fasciculiths decrease notably and progressively below the clay interval, leaving only *F. sidereus, F. thomasii* and *F. tympaniformis* to reach the sequence above it. The demise of the fasciculiths begins 2 m below the benthic extinction event, and accelerates after the deposition of the Ir-rich layer. The evolutionary trend and the three intraspecific variations in *Rhomboaster* described by Angori and Monechi (1996) in the Caravaca section have also been recognised at Zumaya. The LO of *Rhomboaster bramlettei* (with short arms, *R. cuspis* of some authors), which defines the lower boundary of Zone NP10, has been noted just a few centimetres (at $\approx +0.30$ m) below the onset of the dissolution clay (Fig. 7). *R. bramlettei* (with longer arms, probably *R. calcitrapa* and/or *R. bitrifida* of some authors) appears in the middle and upper, slightly calcareous, parts of the clay interval. *R. bramlettei* var. T (more depressed and with a compact structure) occurs just above the clay interval, where also the last *D. araneus* and the first *D. diastypus* were recorded. The LO of *D. diastypus* defines the CP8/CP9 zonal boundary of Okada and Bukry (1980).

The interpretation of our data in terms of the standard calcareous nannofossil zonation of Martini (1971) is based on the understanding of the species of the genus *Rhomboaster* according to Angori and Monechi (1996). Recently, various authors have published different views as to the content of these species and thus the lower boundary of NP10 has been placed differently by these authors (Bybell and Self-Trail, 1995; Angori and Monechi, 1996; Aubry, 1996; Aubry et al., 1996; Wei and Zhong, 1996). Our data suggest that the benthic extinction event took place within early NP10 and in the upper part of CP8.

In other expanded upper Paleocene sections, such as at ODP Hole 690B off Antarctica and Gebel Aweina in Egypt, the benthic extinction event occurs in an interval that has been defined as the middle of Zone NP9 of Martini (1971) (Aubry et al., 1996; Schmitz et al., 1996c). This discrepancy is probably due to the different taxonomic concepts of *R. bramlettei* assumed by the various workers on nannofossils. In Schmitz et al. (1996c) M.-P. Aubry uses the LO of *Tribrachiatus bramlettei* as the base of NP10. Our *R. bramlettei* var. T is similar to specimens of *T. bramlettei* in Aubry et al. (1996, fig. 4, i-l; fig. 3, j,k). If we were to choose the LO of our *R. bramlettei* var. T, or similar forms, as base of NP10, the benthic extinction event would appear to occur in the upper part of NP9 (Fig. 7).

Below the clay interval, the samples include few to common holococcoliths (*Semihololithus biskayae* and *S. kerabyi.*) A shift in the assemblage is evident across the clay interval. Below the clay, the holococcoliths become gradually less common and then disappear completely. This roughly coincides with the greenish marl interval, where the $\delta^{13}C$ values shift to more negative values after a long interval of fairly stable values (Figs. 1 and 2). Above the dissolution clay, holococcoliths are generally rare and representatives of the genus *Braarudosphaera* increase in abundance from the level where the $\delta^{13}C$ values are back to where they were before the dissolution interval.

The subdivision of NP10 proposed by Aubry (1996) could not be recognized, which indicates that the middle part of NP10 is not sampled due to the very short range of *T. digitalis* (the nannofossil sample spacing is about 2 m in this interval), or condensed or missing at Zumaya (Fig. 7). The absence of *T. digitalis* could also be related to palaeoecological or preservational problems.

6. Discussion

6.1. Original isotopic signals?

It is desirable to base reconstructions of past isotopic variations in sea water on analyses of well

preserved, species-determined calcite tests or shells. In the absence of such material, and under certain diagenetic conditions, whole-rock calcite can represent an acceptable alternative, at least for carbon isotopes (see e.g., Corfield et al., 1991; Charisi and Schmitz, 1995). Limestones and marls that have been indurated or compacted during early diagenesis may represent closed systems with respect to carbon isotopes, and therefore have a great potential for retaining original $\delta^{13}C$ signals. The latter is particularly true for sediments where the calcite/organic matter ratio is high (Marshall, 1992), which is almost always the case at Zumaya.

There are some reasons for believing that the general trends of the $\delta^{13}C$ record below and above the dissolution clay at Zumaya represent real oceanic changes. Our bulk-rock isotopic record established on the same type of samples through the rest of the Paleocene at Zumaya shows the same general $\delta^{13}C$ trend as records measured in well-preserved deep-sea material, such as at DSDP Site 577 (see Fig. 4 and Shackleton et al., 1985). The characteristic late Paleocene $\delta^{13}C$ maximum (Corfield, 1994; Thompson and Schmitz, 1997) is well registered at Zumaya. Only three major negative $\delta^{13}C$ shifts are registered: one at the K–T boundary, the benthic extinction event, and the event around the D–S boundary. The first two anomalies have also been found in many other sections worldwide (Corfield, 1994), whereas a D–S boundary anomaly has not been reported before. Only very little attention has previously been focused on the geochemistry of the D–S boundary, and it may be that, so far, this $\delta^{13}C$ anomaly has been overlooked. Further research will show whether it is a global, regional or diagenetic signal (see Schmitz et al., 1996b, for further information on the D–S boundary at Zumaya). Through the rest of the Paleocene at Zumaya, only a few anomalous $\delta^{13}C$ results occur, some of these may reflect diagenetic calcite that we failed to observe. For the isotopic curve in Fig. 4 we have omitted results for samples with visible diagenetic calcite (typically occurring in veins). For example, the values from the dissolution clay within the P–E transition and the calcite vein that marks the K–T boundary (see Margolis et al., 1987) are not included in the figure. Whenever possible (where lithologies are mixed) measurements have been performed on limestone samples rather than on marls. In the dissolution clay above the benthic extinction event the calcite/organic matter ratio may originally have been low and it is likely that the low $\delta^{13}C$ values in this interval at least partially reflect incorporation of carbon from decomposed organic tissue in diagenetic calcite. Decomposing organic matter adds carbon strongly depleted in ^{13}C to the pore water.

Oxygen isotopic ratios in whole-rock are generally much more susceptible to alteration during diagenesis than carbon isotopes (Banner and Hanson, 1990; Marshall, 1992). This is because temperature has a considerably stronger influence during recrystallisation on the isotopic fractionation of oxygen than carbon. There are also many more potential sources of abundant, extraneous oxygen than carbon. The very uniform $\delta^{18}O$ values at the P–E transition above and below the dissolution clay are similar to values measured throughout the rest of the Paleocene section at Zumaya. These values may primarily reflect the environmental conditions during early diagenetic recrystallisation of biogenic calcite. The anomalous and scattered $\delta^{18}O$ values in the dissolution interval suggest a different diagenetic origin for some of this calcite, which is also apparent from visual examinations. At some of the more calcareous levels, however, the $\delta^{18}O$ values are similar to those in the marl–limestones above and below the dissolution clay. For example, one sample in the dissolution clay at +1.5 m ($CaCO_3$=29%) shows a $\delta^{18}O$ value of −4.0‰ (Fig. 3). The $\delta^{13}C$ value in this sample is −1.1‰, which is 2.5‰ lower than in the upper limestone 1.6 m further down in the section. This $\delta^{13}C$ shift has the same magnitude as the shift at the benthic extinction event at ODP Hole 690B. From this perspective it appears reasonable that $\delta^{13}C$ at +1.5 m may reflect original sea-water conditions.

6.2. *The temporal extent of the $\delta^{13}C$ shift at Zumaya*

At Zumaya, the P5 zone, in which the benthic extinction event occurs, spans about 30 m. According to the time scale of Berggren et al.

(1995) the P5 zone represents 1.25 million years. The average sedimentation rate at Zumaya during this time was thus 2.4 cm kyr^{-1}. Turbidites are rare in the P5 interval and no omission surfaces have been found. It is likely that most beds in the section may have formed at rates not too different from the average rate. In the lower clay interval there is almost no calcite and, assuming a constant siliciclastic influx, bulk sedimentation rates for this interval may have been about half of the average; whereas for the upper poorly calcareous parts rates were between 1.2 and 2.4 cm kyr^{-1}. The samples that we think give reliable $\delta^{13}C$ values; that is, the samples that fulfil the three criteria: (1) no visible diagenetic calcite; (2) more than 40% calcite; and (3) 'normal' $\delta^{18}O$ values, indicate that at Zumaya the $\delta^{13}C$ shift ranges over almost 5 m (Fig. 1). The 5 m thick interval may thus correspond to a period of between 200 and 400 kyr. The $\delta^{13}C$ anomaly at ODP Hole 690B, as measured in the benthic foraminifera *N. truempyi,* extends over 2–3 m, and corresponds to 150–200 kyr, according to the sedimentation rate estimates by Kennett and Stott (1991). Given the inherent uncertainties in the sedimentation rate estimates, however, it is still likely that it is the same $\delta^{13}C$ anomaly that is registered at the two sites.

The $\delta^{13}C$ values above the dissolution clay at Zumaya stabilize around 1‰, which is about 0.5‰ lower than the average $\delta^{13}C$ in the interval below the onset of the negative $\delta^{13}C$ excursion (Fig. 1). A similar persistent 0.5‰ negative shift also occurs across the benthic extinction event at ODP Hole 690B (Kennett and Stott, 1991; see plot in Schmitz et al., 1996c). This represents further evidence that limestone and marl whole-rock $\delta^{13}C$ signals at Zumaya are generally reliable.

6.3. *A gradual initiation of the benthic extinction event*

It appears that at Zumaya the negative $\delta^{13}C$ shift associated with the benthic extinction event begins to evolve gradually somewhere between 20 and 40 cm below the base of the dissolution clay (Fig. 2). At ODP 690B the negative $\delta^{13}C$ shift, measured in tests of mid-depth dwelling planktic foraminifera (*Subbotina patagonica*), evolves gradually over about 8 cm (Kennett and Stott, 1991). The *S. patagonica* tests show a 1.5‰ negative shift in the 4 cm interval below the major benthic diversity decline. An additional fall of 0.5‰ occurs in the 4 cm above this level. Kennett and Stott calculated sedimentation rates of 1.2 cm kyr^{-1} for Hole 690B. With sedimentation rates of 2.4 cm kyr^{-1} (i.e., the average P5 sedimentation rate) for the 40 cm of greenish brown marls at Zumaya, this interval corresponds to a time period of $\approx$17 kyr. However, the glauconite maximum in the 10 cm limestone interval just below the marls may represent the 'beginning of the end' for the benthic foraminifera. Moreover, the greenish brown marls may have accumulated faster than the average sediment in the P5 zone. It appears that, whatever environmental change triggered the benthic foraminiferal extinction, this change began 5–20 kyr before the extinction event itself.

There are two palaeontological arguments in favour of the idea that the $\delta^{13}C$ change in the interval just below the benthic extinction event at Zumaya reflects the initiation of the events leading to the extinctions. Firstly, at both ODP Hole 690B and Zumaya there is a small offset in the highest occurrence of *G. beccariiformis* and a major diversity decline in benthic species. At ODP Hole 690B *G. beccariiformis* has its HO 1 cm below the HO of the majority of the other benthics (Kennett and Stott, 1991). At Zumaya there is a 15 cm offset between the HO of *G. beccariiformis* and those of the other benthics (Fig. 6). Secondly, in the calcareous intervals of the dissolution clay an unusual planktic foraminiferal fauna exists, with acarininids, in particular *A. wilcoxensis* and *A. acarinata*, showing major abundance peaks (Fig. 7 and Canudo et al., 1995). These two species, however, show their first strong abundance increase in a sample from the greenish marls at the +0.20 m level (Fig. 7).

The clay dissolution interval may reflect low oxygen conditions at the sea floor, associated with high CO_2 pressure that induced calcite dissolution (Canudo et al., 1995). In the topmost 10 cm of limestone below the greenish marls, glauconite becomes extremely abundant, from having a sparse to rare occurrence in the limestones and marls below. The greenish marls below the dissolution

clay are also very rich in glauconite at many levels but in the clay itself glauconite disappears. Glauconite formation is typically associated with suboxic conditions and such conditions may have preceded more oxygen-deficient conditions when the dissolution clay formed.

6.4. An Ir anomaly of enigmatic origin

There is a possibility that the small Ir anomaly at the base of the greenish marls is related to a physical event, such as the impact of an extraterrestrial body or mafic volcanism emitting Ir-rich aerosols (see Montanari et al., 1993; Schmitz and Asaro, 1996). On the other hand, small Ir anomalies (100–500 ppt) attributed to precipitation of terrestrial Ir from sea or pore water have been found at a number of geological period boundaries and event horizons (Playford et al., 1984; Orth et al., 1986, 1988; Wang et al., 1991, 1993a,b; Schmitz, 1992a). Sedimentation rates at Zumaya in general are far too high for the normal 'background' rain of extraterrestrial dust to be registered (see Peucker-Ehrenbrink, 1996 on cosmic dust influx rates) and there is no sedimentological evidence (e.g., grain size) indicating that the Ir-rich level may represent an extreme condensation level.

We have performed preliminary mineralogical studies and searched the Ir-rich grey layer for shocked quartz, which would represent evidence for that the Ir is impact-related. No shocked quartz was found, although several thousand quartz grains were scanned for shock lamellae. One problem with the shocked quartz search, however, is that the marls in the interval below the benthic extinction event are comparatively coarse grained, with a relatively high amount of ordinary terrestrial quartz grains. If a few shocked quartz grains settled on the sea floor they were admixed with billions of terrestrial quartz grains. Acetic acid leached mineral fractions, >28 μm, from the grey layer appear similar to those from surrounding layers, except for being richer in mica and possibly somewhat more fine-grained. The mica enrichment may reflect fractionation of the thin-flaked grains due to hydrodynamic processes or distal volcanism.

Sediment layers corresponding to boundary levels between geological periods and extinction events generally formed when changes in sea floor environmental conditions or unusual types of sedimentation took place. Redox barriers, related to deposition of abundant organic matter, or representing contact zones between different sedimentary pore water regimes, may therefore typically develop at event levels (see, e.g., Orth et al., 1986, 1988; Schmitz, 1992a,b; Wang et al., 1991, 1993a,b). At the redox barriers different elements, sometimes including Ir, precipitate from pore water. Therefore, small sea-water derived Ir anomalies are probably more common, relatively speaking, at geological period boundaries than in the rest of the geologic column. The Ir anomaly in the grey layer at Zumaya, however, is different from sea-water derived Ir anomalies in so far that it does not show the usual association with typical chalcophile elements such as Se, Sb, and Fe (e.g., Orth et al., 1986, 1988; Schmitz, 1992a; Asaro and Schmitz, unpubl. data). There is nothing in the mineralogy of the grey layer, such as any anomalous amounts of sulphides, ferric hydroxides, organic matter, or phosphates, in support of the idea that precipitation of Ir from sea water has taken place. In the 10 cm thick limestone interval below the grey layer, metal enrichment from sea or pore water took place. Iron, Ni, Co, but not Ir, are enriched in this layer (Fig. 5). It cannot be excluded that the Ir has diffused out of this layer, but one argument against this is that diffusion processes generally lead to a 'bell curve' element pattern, with the peak concentration of the diffused element at its original site. In the strongly Fe- and Co-enriched sample, 5 cm below the grey layer, Ir concentrations are similar to the average for the section. Even if the Ir is sea-water derived it may originally have entered sea-water from volcanism (aerosols) or from a vaporized extraterrestrial body (Schmitz, 1992b).

The Ir anomaly occurs after the onset of the strong glauconite maximum and after beginning of demise in the *Fasciculithus* genus. This indicates that, if the anomaly is related to an impact, the impact may not have been of any deciding consequence for ongoing palaeoceanographic changes and later mass extinctions. Palaeoceanographic and palaeogeographic change may, instead, be

related to, for example, basaltic volcanism, which also may lead to small Ir anomalies (see references in Schmitz and Asaro, 1996). Explosive basaltic volcanism may already have occurred in the northernmost part of the Atlantic at this time (Schmitz and Heilmann-Clausen, unpubl. data) but the main phase of tholeiitic volcanism during the Greenland–Eurasia separation occurred much later (Berggren and Aubry, 1996; Schmitz and Asaro, 1996; Schmitz et al., 1996a). Although a small or medium sized extraterrestrial body is a possible source of the Ir enrichment at Zumaya, further detailed studies, involving other sections across the benthic extinction event, are necessary in order to determine its origin.

7. Summary

High-resolution bulk-rock isotopic, trace element and micropalaeontological studies were performed across the latest Paleocene benthic extinction event at Zumaya, Spain. A bulk-rock $\delta^{13}C$ profile over the entire Paleocene at this site was also made. The great similarity in the $\delta^{13}C$ records between Zumaya and deep-sea sites with well preserved sediments suggest that the $\delta^{13}C$ results at Zumaya reflect original conditions and can be used for correlation.

The benthic extinction event occurs at the base of a 4 m thick interval with no or little calcite, the 'dissolution clay'. In the marls in the 40 cm interval immediately below and in the 1 m interval just above the clay a fall and a rise, respectively, in $\delta^{13}C$ is registered, representing probably the initial and the final stage of the global $\delta^{13}C$ excursion associated with the benthic extinction event. In total, the negative $\delta^{13}C$ values span a 5 m thick interval, which probably corresponds to 200–400 kyr. This time interval is of the same order of magnitude as the estimated duration, 150–200 kyr, of the $\delta^{13}C$ excursion observed at ODP Hole 690B. The difference between the two estimates can be accounted for by uncertainties in the sedimentation rate calculations.

The following sequence of change is registered through the latest Paleocene–earliest Eocene at Zumaya: A decline in *Fasciculithus* abundance and gradual changes in planktic foraminifera fauna occur a few meters below the base of the dissolution clay. In the interval from 50 to 40 cm below the base of the dissolution clay glauconite becomes very abundant. In a 1 cm thick grey marl layer about 40 cm below the base of the dissolution clay, a significant Ir anomaly occurs (133 ppt over a background of 38 ppt) of enigmatic origin. Above the Ir anomaly follows $\approx$40 cm of glauconitic, greenish brown marls through which a gradual, 1.6‰ negative $\delta^{13}C$ excursion is developed. The greenish brown marls probably represent a time interval of 10–20 kyr. In these marls the demise in the *Fasciculithus* genus accelerates, and the first of the typical late Paleocene benthic foraminifera, *G. beccariiformis*, becomes extinct. Acarininids show an increase in abundance in the upper part of the marls. Where the greenish brown marls pass into clay, devoid of original calcite, a large number of the typical late Paleocene deep-sea benthic foraminifera disappear. At calcareous levels in the middle part of the 4 m of dissolution clay an unusual planktic foraminifera fauna occurs, dominated by acarininid foraminifera. In connection with return of marl deposition, $\delta^{13}C$ gradually increases and then stabilizes at values about 0.5‰ lower than before the isotopic excursion. The extinction of the *Fasciculithus* genus is registered somewhat after the $\delta^{13}C$ values have returned to pre-excursion values. After this, more normal conditions, with alternating marls and limestones, and a stable $\delta^{13}C$ trend are registered.

The gradual sequence of environmental change in the 50 cm below the dissolution clay, are more readily reconciled with changing oceanic circulation and rearranged palaeogeography, possibly in connection with volcanism, rather than an instantaneous triggering event, such as an extraterrestrial body impact. The small Ir anomaly found may reflect such volcanism, sea-water precipitates, or it may reflect a small impact event coincident with environmental change, but possibly of no consequence to the change already in progress.

Acknowledgements

This study was supported by the Bank of Sweden Tercentenary Foundation, Erna and Victor

Hasselblad Foundation, Futura, Magnus Bergvalls Foundation, Swedish Institute, Wenner-Gren Foundations, Swedish Natural Science Research Council and DGICYT project PB94-0566. We thank O. Gustafsson for the isotopic analyses, and R. Corfield, D. Pak, and F. Surlyk for helpful reviews. This is a contribution to IGCP Project 308.

References

Angori, E., Monechi, S., 1996. High-resolution nannofossil biostratigraphy across the Paleocene/Eocene boundary at Caravaca (southern Spain). Israel J. Earth Sci. 44, 197–206.

Arenillas, I., Molina, E., 1996. Bioestratigrafia y evolución de las asociaciones de foraminíferos planctónicos del transito Paleoceno–Eoceno en Alamedilla (Cordilleras Béticas). Rev. Esp. Micropaleontol. 18, 76–96.

Aubry, M.P., 1996. Towards an upper Paleocene–lower Eocene high resolution stratigraphy based on calcareous nannofossil stratigraphy. Israel J. Earth Sci. 44, 239–253.

Aubry, M.-P., Berggren, W.A., Stott, L., Sinha, A., 1996. The upper Paleocene–lower Eocene stratigraphic record and the Paleocene–Eocene boundary carbon isotope excursion. In: Knox, R.W.O'B. et al. (Eds.), Correlation of the Early Paleogene in Northwest Europe. Geol. Soc. London Spec. Publ. 101, 353–380.

Banner, J.L., Hanson, G.N., 1990. Calculation of simultaneous isotopic and trace element variations during water–rock interaction with applications to carbonate diagenesis. Geochim. Cosmochim. Acta 54, 3123–3137.

Barron, E.J., Peterson, W.H., 1991. The Cenozoic ocean circulation based on ocean General Circulation Model results. Palaeogeogr. Palaeoclimatol. Palaeoecol. 83, 1–28.

Berggren, W.A., Aubry, M.P., 1996. A late Paleocene–early Eocene NW European and North Sea magnetobiochronological correlation network. In: Knox, R.W.O'B. et al. (Eds.), Correlation of the Early Paleogene in Northwest Europe. Geol. Soc. London Spec. Publ. 101, 309–352.

Berggren, W., Miller, K.G., 1988. Paleogene planktonic foraminiferal biostratigraphy and magnetobiochronology. Micropaleontology 34, 362–380.

Berggren, W.A., Kent, D.V., Swisher, C., Aubry, M.P., 1995. A revised Paleogene geochronology and chronostratigraphy. In: Berggren, W.A. et al. (Eds.), Geochronology, Time Scales, and Global Stratigraphic Correlation: Framework for an Historical Geology. SEPM Spec. Publ. 54, 129–212.

Bolli, H.M., Saunders, J.B., Perch-Nielsen, K., 1985. Plankton Stratigraphy. Comparison of Zonal Schemes for Different Fossil Groups. Vol. 1. Cambridge University Press, pp. 3–10.

Bralower, T.J., Mutterlose, J., 1995. Calcareous nannofossil biostratigraphy of Site 865, Allison Guyot, central Pacific Ocean: A tropical Paleogene reference section. Proc. Ocean Drill. Prog., Sci. Results 143, 31–73.

Bybell, L.M., Self-Trail, J.M., 1995. Evolutionary, biostratigraphic, and taxonomic study of calcareous nannofossils from a continuous Paleocene/Eocene boundary section in New Jersey. U.S. Geol. Surv. Prof. Pap. 1554, 1–36.

Canudo, J.I., Molina, E., 1992. Planktic foraminiferal faunal turnover and bio-chronostratigraphy of the Paleocene - Eocene boundary at Zumaya, northern Spain. Rev. Soc. Geol. Esp. 5, 145–157.

Canudo, J.I., Keller, G., Molina, E., Ortiz, N., 1995. Planktic foraminiferal turnover and $\delta^{13}C$ isotopes across the Paleocene–Eocene transition at Caravaca and Zumaya, Spain. Palaeogeogr. Palaeoclimatol. Palaeoecol. 114, 75–100.

Charisi, S.D., Schmitz, B., 1995. Stable ($\delta^{13}C$, $\delta^{18}O$) and strontium ($^{87}Sr/^{86}Sr$) isotopes through the Paleocene at Gebel Aweina, eastern Tethyan region. Palaeogeogr. Palaeoclimatol. Palaeoecol. 116, 103–129.

Corfield, R.M., 1994. Palaeocene oceans and climate: An isotopic perspective. Earth-Sci. Rev. 37, 225–252.

Corfield, R.M., Cartlidge, J.E., Premoli-Silva, I., Housley, R.A., 1991. Oxygen and carbon isotope stratigraphy of the Paleogene and Cretaceous limestones in the Bottaccione Gorge and Contessa Highway sections Umbria, Italy. Terra Nova 3, 414–422.

El Mamoune, B., Martinez-Gallego, J., 1995. Calcareous nannofossils and planktic foraminifera of the Paleocene–Eocene boundary of Southern Spain. In: Flores, J.A., Sierro, F.J. (Eds.), Proc. 5th INA Conf. Salamanca. Universidad de Salamanca, pp. 143–161.

Eldholm, O., Thomas, E., 1993. Environmental impact of volcanic margin formation. Earth Planet. Sci. Lett. 117, 319–329.

Kaiho, K., 1994. Planktonic and benthic foraminiferal extinction events during the last 100 m.y.. Palaeogeogr. Palaeoclimatol. Palaeoecol. 111, 45–71.

Kelly, D.C., Bralower, T.J., Zachos, J.C., Premoli-Silva, I., Thomas, E., 1996. Rapid diversification of planktonic foraminifera in the tropical Pacific (ODP Site 865) during the late Paleocene thermal maximum. Geology 24, 423–426.

Kennett, J.P., Stott, L.D., 1991. Abrupt deep-sea warming, paleoceanographic changes and benthic extinctions at the end of the Paleocene. Nature 353, 225–229.

Knox, R.W.O'B., Morton, A.C., 1988. The record of early Tertiary N. Atlantic volcanism in sediments of the North Sea Basin. In: Morton, A.C., Parson, L.M. (Eds.), Early Tertiary Volcanism and the Opening of the NE Atlantic. Geol. Soc. London Spec. Publ. 39, 407–419.

Lu, G., Keller, G., 1995. Ecological stasis and saltation: species richness change in planktic foraminifera during the late Paleocene to early Eocene, DSDP Site 577. Palaeogeogr. Palaeoclimatol. Palaeoecol. 117, 211–227.

Margolis, S.V., Mount, J.F., Dohne, E., Showers, W., Ward, P., 1987. The Cretaceous/Tertiary boundary carbon and oxygen isotope stratigraphy, diagenesis, and paleoceanography at Zumaya, Spain. Paleoceanography 2, 361–377.

Marshall, J.D., 1992. Climatic and oceanographic isotopic signals from the carbonate rock record and their preservation. Geol. Mag. 129, 143–160.

Martini, E., 1971. Standard Tertiary and Quaternary calcareous nannoplankton zonation. In: Proc. 2nd Planktonic Conf., Rome, 1970, pp. 739–785.

Michel, H.V., Asaro, F., Alvarez, W., 1991. Geochemical study of the Cretaceous–Tertiary boundary region in ODP Hole 752B. Proc. Ocean Drill. Prog. Sci. Results 121, 415–422.

Molina, E., 1994. Paleocene sections in Spain: Chronostratigraphical problems and possibilities. GFF 116, 58–60.

Molina, E., Canudo, J.I., Martínez-Ruiz, F., Ortiz, N., 1994. Integrated stratigraphy across the Paleocene/Eocene boundary at Caravaca, southern Spain. Eclog. Geol. Helv. 87 (1), 47–61.

Molina, E., Arenillas, I., Schmitz, B., 1996. Field trip guide to the Paleocene and lower Eocene of the Zumaya section. in: Proc. Conf. Early Paleogene Stage Boundaries, Zaragoza, pp. 57–72.

Monechi, S., Angori, E., 1996. Toward a better definition of the Paleocene/Eocene boundary: new calcareous nannofossil results from the Zumaya and Caravaca sections. In: Proc. Conf. Early Paleogene Stage Boundaries, Zaragoza, p. 31.

Montanari, A., Asaro, F., Michel, H.V., Kennett, J.P., 1993. Iridium anomalies of Late Eocene age at Massignano (Italy), and ODP Site 689B (Maud Rise, Antarctic). Palaios 8, 420–437.

Okada, H., Bukry, D., 1980. Supplementary modification and introduction of code numbers to the low-latitude coccolith biostratigraphic zonation (Bukry, 1973, 1975). Mar. Micropaleontol. 5, 321–325.

Orth, C.J., Quintana, L.R., Gilmore, J.S., Grayson, R.C., Jr., Westergaard, E.H., 1986. Trace-element anomalies at the Mississippian/Pennsylvanian boundary in Oklahoma and Texas. Geology 14, 986–990.

Orth, C.J., Quintana, L.R., Gilmore, J.S., Barrick, J.E., Haywa, J.N., Spesshardt, S.A., 1988. Pt-group metal anomalies in the Lower Mississippian of southern Oklahoma. Geology 16, 627–630.

Ortiz, N., 1995. Differential patterns of benthic foraminiferal extinctions near the Paleocene/Eocene boundary in the North Atlantic and the western Tethys. Mar. Micropaleontol. 26, 341–359.

Pak, D.K., Miller, K.G., 1992. Paleocene to Eocene benthic foraminiferal isotopes and assemblages: implications for deepwater circulation. Paleoceanography 7, 405–422.

Peucker-Ehrenbrink, B., 1996. Accretion of extraterrestrial matter during the last 80 million years and its effect on the marine osmium isotope record. Geochim. Cosmochim. Acta 60, 3187–3196.

Playford, P.E., McLaren, D.J., Orth, C.J., Gilmore, J.S., Goodfellow, W.D., 1984. Iridium anomaly in the Upper Devonian of the Canning Basin, Western Australia. Science 226, 437–439.

Pujalte, V., Robles, S., Robador, A., Baceta, J.L., Orue-Etxebarria, X., 1993. Shelf-to-basin Palaeocene palaeogeography and depositional sequences, western Pyrenees, north Spain. Spec. Publ. Int. Assoc. Sedimentol. 18, 369–395.

Schmitz, B., 1988. Origin of microlayering in worldwide distributed Ir-rich marine Cretaceous/Tertiary boundary clays. Geology 16, 1068–1072.

Schmitz, B., 1992a. An iridium anomaly in the Ludlow Bone Bed from the Upper Silurian. Geol. Mag. 129, 359–362.

Schmitz, B., 1992b. Chalcophile elements and Ir in continental Cretaceous–Tertiary boundary clays from the western interior of the USA. Geochim. Cosmochim. Acta 56, 1695–1703.

Schmitz, B., Asaro, F., 1996. Iridium geochemistry of volcanic ash layers from the early Eocene rifting of the northeastern North Atlantic and some other Phanerozoic events. Geol. Soc. Am. Bull. 108, 489–504.

Schmitz, B., Heilmann-Claussen, C., King, C., Steurbaut, E., Andreasson, F.P., Corfield, R.M., Cartlidge, J.E., 1996a. Stable isotope and biotic evolution in the North Sea during the early Eocene: the Albaek Hoved section, Denmark. In: Knox, R.W.O'B. et al. (Eds.), Correlation of the Early Paleogene in Northwest Europe. Geol. Soc. London Spec. Publ. 101, 275–306.

Schmitz, B., Molina, E., Von Salis, K., 1996b. The Zumaya section in Spain: A possible global stratotype section for the Selandian and Thanetian stages. Newsl. Stratigr., in press.

Schmitz, B., Speijer, R.P., Aubry, M.-P., 1996c. The latest Paleocene benthic extinction event on the southern Tethyan shelf (Egypt): Foraminiferal stable isotopic ($\delta^{13}C$, $\delta^{18}0$) records. Geology 24, 347–350.

Shackleton, N.J., Hall, M.A., Bleil, U., 1985. Carbon-isotope stratigraphy, Site 577. Init. Rep. Deep Sea Drill. Proj. 86, 503–511.

Speijer, R.P., van der Zwaan, G.J., 1994 The differential effect of the Paleocene–Eocene boundary event: extinction and survivorship in shallow to deep water Egyptian benthic foraminiferal assemblages. In: Speijer, R.P. (Ed.), Extinction and Recovery Patterns in Benthic Foraminiferal Paleocommunities Across the Cretaceous–Paleogene and Paleocene–Eocene Boundaries. Ph.D. Thesis, Utrecht Univ., Geol. Ultraiectina, 124, 121–168.

Speijer, R.P., van der Zwaan, G.J., Schmitz, B., 1996a. The impact of Paleocene–Eocene boundary events on middle neritic benthic foraminiferal assemblages from Egypt. Mar. Micropaleontol. 28, 99–132.

Speijer, R.P., Schmitz, B., Aubry, M.-P., Charisi, S.D., 1996b. The latest Paleocene benthic extinction event: Punctuated turnover in outer neritic foraminiferal faunas from Gebel Aweina, Egypt. Isr. J. Earth Sci. 44, 207–222.

Thomas, E., 1990. Late Cretaceous–early Eocene mass extinctions in the deep sea. Geol. Soc. Am. Spec. Pap. 247, 481–495.

Thomas, E., Shackleton, N.J., 1996. The latest Paleocene benthic foraminiferal extinction and stable isotope anomalies. In: Knox, R.W.O'B. et al. (Eds.), Correlation of the early Paleogene in Northwest Europe. Geol. Soc. London Spec. Publ. 101, 401–441.

Thompson, E.I., Schmitz, B., 1997. Barium and the late Paleocene $\delta^{13}C$ maximum: Evidence of increased oceanic surface productivity. Paleoceanography 12, 239–254.

Tjalsma, R.C., Lohmann, G.P., 1983. Paleocene–Eocene

bathyal and abyssal foraminifera from the Atlantic Ocean. Micropaleontol. Spec. Publ. 4, 94

Wang, K., Orth, C.J., Attrep, M., Jr., Chatterton, B.D.E., Hou, H., Geldsetzer, H.J.H., 1991. Geochemical evidence for a catastrophic biotic event at the Frasnian/Famennian boundary in south China. Geology 19, 776–779.

Wang, K., Attrep, M., Jr., Orth, C.J., 1993a. Global iridium anomaly, mass extinction, and redox change at the Devonian–Carboniferous boundary. Geology 21, 1071–1074.

Wang, K., Orth, C.J., Attrep, M., Jr., Chatterton, B.D.E., Wang, X., Li, J., 1993b. The great latest Ordovician extinction on the South China Plate: Chemostratigraphic studies of the Ordovician–Silurian boundary interval on the Yangtze Platform. Palaeogeogr. Palaeoclimatol. Palaeoecol. 104, 61–79.

Wedepohl, K., 1995. The composition of the continental crust. Geochim. Cosmochim. Acta 59, 1217–1232.

Wei, W., Zhong, S., 1996. Taxonomic and magnetobiochronology of *Tribrachiatus* and *Rhomboaster*, two genera of calcareous nannofossils. J. Palaeontol. 70, 7–22.